Direct observation of OH photofragment from triplet hydroxyacetone

ARTICLE *in* CHEMICAL PHYSICS LETTERS · APRIL 2002

Impact Factor: 1.9 · DOI: 10.1016/S0009-2614(02)00391-3

4 AUTHORS, INCLUDING:

Pradyot Chowdhury

19 PUBLICATIONS **176** CITATIONS

SEE PROFILE

Jai Pal Mittal

Bhabha Atomic Research Centre

259 PUBLICATIONS **3,202** CITATIONS

SEE PROFILE

26 April 2002

Chemical Physics Letters 356 (2002) 476–482

CHEMICAL PHYSICS LETTERS

www.elsevier.com/locate/cplett

Direct observation of OH photofragment from triplet hydroxyacetone

Pradyot K. Chowdhury *, Hari P. Upadhyaya, Prakash D. Naik, Jai P. Mittal

Radiation Chemistry & Chemical Dynamics Division, Bhabha Atomic Research Centre, Trombay, Mumbai 400 085, India

Received 19 December 2001; in final form 28 February 2002

Abstract

In contrast to the photoexcitation of hydroxyacetone (HA) at 193 nm resulting in an instantaneous dissociation of the Rydberg $^1(n, 3s)$ state, on photoexcitation at 248 nm the singlet $^1(n, \pi^*)$ excited HA molecule first undergoes intersystem crossing (ISC) to the triplet state, followed by a minor dissociation channel to CH_3COCH_2 and OH radicals. The real time formation of OH, which is probed by laser-induced fluorescence (LIF), shows a rate constant to be $\geqslant 10^8$ s^{-1}. The initial rotational state distribution of OH ($X^2\Pi$) is found to be Boltzmann-like, characterized by a single rotational temperature T_{rot} of 450 ± 40 K. The average relative translational energy of the photofragments is determined by Doppler spectroscopy to be 8.7 ± 2.0 kcal mol^{-1}. The observation of OH with a modest rotational energy, no vibrational energy, and a large amount of translational energy suggests significant exit energy barrier with the dissociating surface. © 2002 Published by Elsevier Science B.V.

1. Introduction

The photophysics and photochemistry of acetone is well investigated [1–6]. By replacing a H-atom in acetone by OH, the photophysics may remain same, however, the possibility of studying interesting photochemistry opens up. Similar to acetone, hydroxyacetone (HA) has two absorption bands, a broad weak band at 266 nm due to the $^1(n, \pi^*)$ transition and a strong band in the 180–195 nm region due to $^1(n, 3s)$ transition. Recently, the steady state photodissociation study of HA at 266 nm band is reported [7]. The primary dissociation step is C–C bond rupture, as is observed for acetone:

$$CH_3COCH_2OH \rightarrow COCH_2OH + CH_3 \quad (1a)$$

$$\rightarrow CH_3CO + CH_2OH \quad (1b)$$

We have recently reported [8] HA pump-probe study at 193 nm excitation, where the Rydberg excited $^1(n, 3s)$ CH_3COCH_2OH udergoes instantaneous α-cleavage, followed by secondary dissociation of $CH_2OH/COCH_2OH$ to generate OH which is probed by laser induced fluorescence (LIF). While the threshold dissociation energy of $CH_2OH \rightarrow CH_2 + OH$ as 100 kcal mol^{-1}, refutes this as a viable mechanism, nevertheless CO $CH_2OH \rightarrow COCH_2 + OH$ is energetically feasible, with a $\Delta H = 36$ kcal mol^{-1}. The observation of the

* Corresponding author. Fax: +91-22-5505-151.

E-mail addresses: pkc@apsara.barc.ernet.in, cpradyot@yahoo.com (P.K. Chowdhury).

0009-2614/02/$ - see front matter © 2002 Published by Elsevier Science B.V.
PII: S0009-2614(02)00391-3

OH formation rate constant of 5×10^6 s^{-1} from the dissociation of $COCH_2OH$ vis-a-vis RRKM calculations, suggested that the $COCH_2OH$ radical was formed with less than 2 kcal mol^{-1} of excess energy above its dissociation threshold. Thus, the secondary dissociation producing OH is not expected with the irradiation of HA at 248 nm.

We report here the real time formation of OH, monitored by LIF, with a rate constant, $k \geqslant 10^8$ s^{-1} on irradiation of HA at 248 nm. While the energy barrier on the singlet excited surface prohibits its dissociation, the vibrationally excited ground electronic state HA, if formed by internal conversion, would be dissociating at a RRKM predicted rate of 10^4 s^{-1}. Therefore, it appears that the singlet $^1(n,\pi^*)$ excited HA undergoes intersystem crossing (ISC) to the triplet state, followed by dissociation generating CH_3COCH_2 and OH radicals as a minor channel, in addition to two major C–C bond rupture channels ((1a) and (1b)) mentioned above. The OH radical has a rich rotational spectroscopy and is suitable for the determination of product energy distributions. Some dynamic information on the dissociation reaction can be obtained from the nascent initial state distribution of the products, e.g., $OH(v,N,f)$, where v is the vibrational quantum number, N is the rotational quantum number, and f refers to one of the four OH fine structure levels. The observation of OH with very little rotational energy and with no vibrational energy, but with a significant translational energy suggests its formation from the triplet surface with a significant exit energy barrier.

2. Experimental

The schematic of the laser photolysis-laser induced fluorescence setup (LP-LIF) used in the present study and the experimental procedures are given in our earlier publications [8–10], a brief account is as follows. The photolysis laser employed is an excimer laser (Lambda Physik Model Compex-102, Fluorine version) and the probe laser is Quantel dye laser with frequency doubling and mixing module (TDL 90) pumped by Quantel seeded Nd:YAG laser (model YG 980 E-20). The reaction chamber is made up of stainless steel with crossed right angle arms for photolysis and probe lasers. All the arms are equipped with baffles and the windows are fixed at the Brewster angle to decrease scattering. The photolysis and the probe lasers intersect at the centre of the reaction cell. The detection system views at right angle the intersection volume of photolysis and probe laser through the bottom arm window. The fluorescence is collected by a 38 mm diameter lens of focal length 50 mm, and detected by a PMT (Hamamatsu model R 928P). A band pass filter ($\lambda_{centre} = 310$ nm, FWHM $= \pm 10$ nm, $\%T_{310\ nm} = 10\%$) is placed between the collecting lens and the PMT to cut-off the scattering from the photolysis laser. The fluorescence signal is gate integrated by a boxcar (SRS 250), averaged for 30 laser shots and fed into an interface (SRS 245) for A/D conversion. A Pentium II PC is used to control the scan of the dye laser via RS232 interface and to collect data through GPIB interface using control and data acquisition program. To correct for the laser intensity fluctuations, both the pump and the probe lasers are monitored by photodiodes and fluorescence intensities are normalized.

In the present work, the HA vapour is flowed through the reaction chamber at a flow velocity of approximately 10 cm s^{-1} and photolyzed at 248 nm. The HA pressure is maintained at about 100 mTorr. The OH fragment is probed state selectively by exciting $A^2\Sigma \leftarrow X^2\Pi$ $(0,0)$ transition of OH (306–309 nm) and monitoring the subsequent $A \rightarrow X$ fluorescence. The laser frequency was calibrated using the optogalvanic signal of a hollow-cathode lamp with an accuracy of ± 0.3 cm^{-1}. The spectral resolution of the probe laser is 0.06 cm^{-1}. Both the laser beams used are unfocused and attenuated further to prevent saturation. The measured LIF signal is found to be linearly proportional to the laser power. HA (95% purity, Fluka) is known to be hygroscopic and required dehydration prior to use. A 10 ml sample was pumped on at room temperature for 5 h before use.

3. Results and discussion

Since the photodissociation mechanism of HA is not clearly known, one may get insights from the studies of acetone [11–15]. At lower energies of the

$^1(n,\pi^*)$ absorption band, the dominant relaxation process in excited state acetone is ISC, from the first excited singlet S_1 to the lowest triplet T_1, with an ISC rate [11] about 3×10^8 s^{-1}. Strong evidences of dissociation to $CH_3 + COCH_3$ from the triplet surface have been reported [12,13]. Recently, the barrier heights for the dissociation on the T_1 surface have been measured to be 13.4 kcal mol^{-1} [14]. The presence of an exit barrier in the dissociation of carbonyl-containing molecules has been generally observed, with a high fraction of available energy appeared in fragment translation. A recent theoretical calculation [15] has shown that the higher barrier heights for the dissociation on S_1 surface than that of the triplet T_1 surface, prohibits its dissociation from S_1 state. Although dissociation to $H + CH_2COCH_3$ requires much more energy [16] in acetone, the energetics of the HA dissociation to $OH + CH_2COCH_3$ is close to that of the α-cleavages. Thus, the first step of the photodissociation of HA is C–C or C–O bond rupture [17–19] as follows:

$$CH_3COCH_2OH \rightarrow COCH_2OH + CH_3 \qquad \Delta H^0 = 80 \text{ kcal mol}^{-1} \quad (1a)$$

$$\rightarrow CH_3CO + CH_2OH \qquad \Delta H^0 = 80 \text{ kcal mol}^{-1} \quad (1b)$$

$$CH_3COCH_2OH \rightarrow CH_3COCH_2 + OH \qquad \Delta H^0 = 90 \text{ kcal mol}^{-1} \quad (2)$$

We observed OH formation within 20 ns of the 248 nm KrF laser pulse at a pressure of 100 mTorr HA; where the secondary dissociation of radicals are energetically not accesible. The threshold dissociation energy of $CH_2OH \rightarrow CH_2 + OH$ is 100 kcal mol^{-1}, and that of $COCH_2OH \rightarrow COCH_2 + OH$ is 36 kcal mol^{-1}, refutes them as a viable mechanism. The fast OH formation appears to be from the triplet surface of HA by surpassing an energy barrier. The measured Doppler profile of OH (cf. Section 3.2) suggests an exit barrier of 9.2 kcal mol^{-1}. By considering the endothermicity of 10 kcal mol^{-1}, the barrier height for the OH dissociation on triplet HA has been evaluated to be 19.2 kcal mol^{-1}. Assuming that both the reaction channels 1 and 2 are opening up from the triplet HA with barrier heights of 13.4 and 19.2 kcal mol^{-1}, respectively, RRKM calculation gives the branching ratio for OH forming path (channel 2) to be about 3%.

3.1. Rotational state distribution of nascent OH by LIF

The formation of OH radicals was observed in the irradiation of HA by a pulsed KrF excimer laser. Typical LIF signals from OH exhibited simple exponential decays, with decay times consistent with OH $A^2\Sigma^+$ state measurements. A typical LIF spectrum of OH observed at a probe time of 50 ns after the excimer laser pulse and a HA pressure of 100 mTorr is shown in Fig. 1. At this pressure, the hard-sphere collision rate is 10^6 s^{-1} molecule^{-1}, which ensures that no collisional relaxation occurred within the probe time of 50 ns. The line assignment and nomenclature are based on the extensive spectroscopic work of Dieke and Crosswhite [20]. All the peaks in Fig. 1 correspond to transitions originating in the $X^2\Pi_i$ $(v = 0)$ level. Normally, relative peak areas of the rotational lines of LIF signals were used to obtain relative OH densities. Conversion of the measured LIF signal S to a state-resolved $OH(X^2\Pi)$ population requires correction for variations in the intensity of both the KrF and probe lasers I_{photol} and

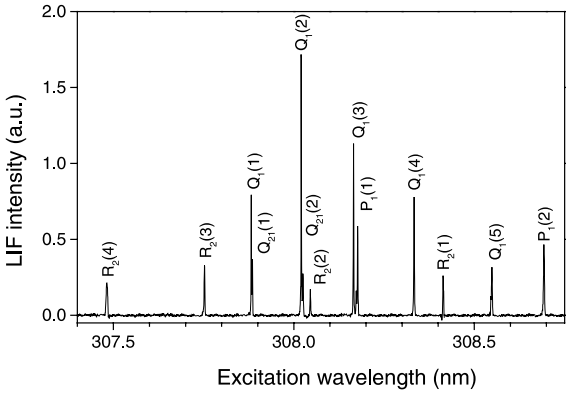

Fig. 1. Portion of the LIF rotational excitation spectrum of OH radical formed in the irradiation of HA by a KrF excimer laser (20 ns, 150 mJ/pulse). The HA pressure used is 100 mTorr, and the delay between the KrF and the dye laser is 50 ns. The spectral assignments are based on [20].

I_{probe}, as well as accurate values of the Einstein coefficients, B_{ik} for the k $\leftarrow$ i transition at ν_{ik}.

$$P(v'', N'', f'', \lambda'') = \frac{S}{I_{\text{photol}} I_{\text{probe}} B_{\text{ik}} \nu_{\text{ik}}}. \quad (1)$$

The pump and probe laser intensity variation was monitored simultaneously with the LIF signal during spectral scan. Tabulated values of B_{ik} are used throughout [21]. Here, the energy of the analysis laser (maximum energy about 10 mJ/pulse) was reduced by a factor of 1000 to ensure a linear response of the fluorescence to laser power. Conversion of the spectrum to micropopulations is obtained by dividing the state populations by their rotational degeneracy, $(2J'' + 1)$. A Boltzmann plot of rotational states, i.e., in $[P(J)/(2J + 1)]$ vs E_R, the rotational energy of the state, is shown in Fig. 2. The straight line is the computer least-squares fit of the data, representing different lambda $(^2\Pi^+, ^2\Pi^-)$ and spin $(^2\Pi_{3/2}, ^2\Pi_{1/2})$ states. They seem to have approximately the same Boltzmann distribution, characterized by a common rotational temperature (T_R) of 450 ± 40 K. This measured distribution of initial rotational states correspond to an average rotational energy in OH, $E_R = 0.9$ kcal mol^{-1}. A second set of experiment was carried out to cross-check and determine $P(J)$ for OH$(^2\Pi)$ states, which gave an identical result for T_R.

To see whether any OH is produced in the $v'' = 1$ level, the R_1 band-head of the (1,1) vibrational transition was scanned. No OH$(v'' = 1)$ could be observed, even when using higher excimer laser output (energy fluence = 20 mJ cm^{-2}) and increasing the probe laser intensity a factor of 10. The signal-to-noise ratio in the LIF excitation spectra was such that the failure to observe the (1,1) R_1 branch means that the population ratio in the $v'' = 0$ was at least 100 times greater than the $v'' = 1$.

3.2. Translational energy of OH from Doppler line-width

The component of OH fragment velocity along the probe laser propagation axis z, v_z, shifts the central absorption frequency ν_0 to ν by the following equation:

$$\nu = \nu_0(1 \pm v_z/c), \quad (2)$$

where c is the velocity of light. The linewidth and shape of the Doppler broadened LIF line includes contributions from the fragment molecular velocity, the thermal motion of the parent and the finite probe laser line-width. The peak profile for $P_1(2)$ is shown in Fig. 3. All the rotational lines are seen to exhibit the same line-width within the experimental error. For a completely isotropic OH fragment

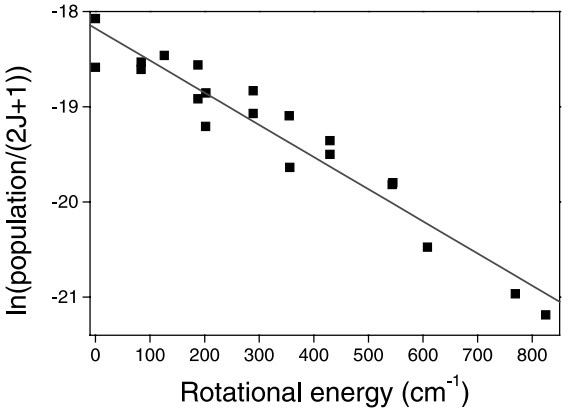

Fig. 2. Boltzmann plot of the populations in various microstates of nascent OH. The distribution of four different spin and Λ-doublet states of OH is characterized by a temperature $T^R = 450 \pm 40$ K.

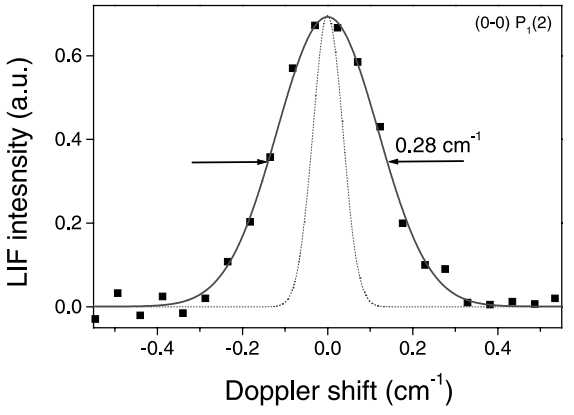

Fig. 3. Doppler profile of the $P_1(2)$ line in the spectrum. The solid line drawn through the data points represents a Gaussian fit to the data points. The dotted line represents the instrument function (FWHM = 0.07 cm^{-1}).

velocity distribution, the deconvolution of the peak profiles with the instrumental function gives the Doppler width to be 0.27 ± 0.03 cm^{-1}. For the Maxwell–Boltzmann translational energy distribution, this corresponds to an average translational energy of 8.7 ± 2.0 kcal mol^{-1} in the photofragments center of mass coordinate. The OH velocity distribution is expected to be very broad as its recoil partner CH_3COCH_2 has high density of internal states. We have assumed a Gaussian profile for the velocity distribution which fits quite well with the observed velocity distribution. The release of significant translational energy with the products suggest that there is an exit barrier. The exit barrier height is equivalent to the activation energy required for the recombination of the products, $CH_3COCH_2 + OH$ and approximately 95% of it is released as the translational energy with the dissociation products [9]. Since we have observed an average translational energy of 8.7 ± 2.0 kcal mol^{-1} in the photofragments, about 9.2 ± 2.0 kcal mol^{-1} may be considered as the exit energy barrier for the triplet HA producing $CH_3COCH_2 + OH$.

In another study, the 193 nm ArF excimer laser radiation was varied from 2 to 20 mJ/pulse and the OH LIF intensity of the $Q_1(3)$ rotational line was monitored as a function of the excimer laser fluence. The log–log plot of LIF signal vs photolysis energy yields a slope of 0.9 ± 0.1. This indicates that the OH radicals are produced in a single-photon process.

3.3. Dissociation dynamics of CH_3COCH_2OH

The production of $OH(v'' = 0)$ as a function of the delay time between the two lasers was obtained by monitoring the intensity of the $Q_1(3)$ LIF signal as shown in Fig. 4A. The buildup of the signal was found to be instanteneous during a few tens of nanoseconds within the photolysis laser pulse, whereas its slow decay was observed few microsecond afterwards. Fig. 4B is given for comparison, which exibits the slow formation of OH from the secondary dissociation of $COCH_2OH$ radical generated by ArF laser irradiation of HA [8]. The first data point was taken at a probe laser fired 500 ns before the photolysis laser, and subsequent data

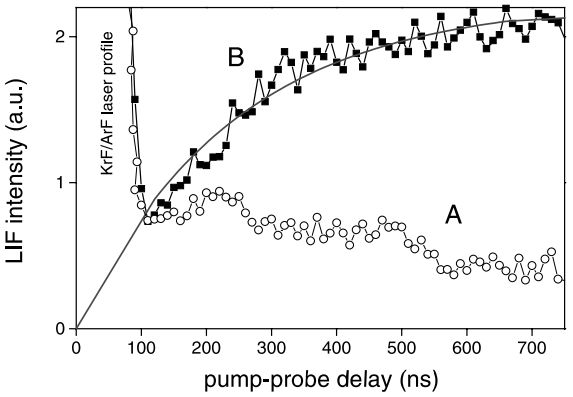

Fig. 4. (A) LIF intensity of OH generated in the dissociation of CH_3COCH_2OH as a function of the pump-probe delay. The HA pressure is 100 mTorr and the KrF laser fluence is 2 mJ cm^{-2}. (B) is given for comparison, where slow formation of OH is observed earlier from the secondary dissociation of $COCH_2OH$ radical generated by ArF laser irradiation of HA [8].

points taken at 10 ns intervals afterwards, which are averaged over 100 pulses. The measurement was carried out at a HA pressure of 100 mTorr and at a KrF laser fluence of 2 mJ cm^{-2}. Several other intense rotational lines, mainly the strong lines of the Q_1 and P_1 branch of the $(0,0)$ transition, were also measured as a function of the delay. It was found that the time-dependent signal intensities were independent of the rotational lines probed (2, 4 or 5). This suggests that no significant rotational relaxation occurs on the above time scale. The fast buildup of the OH signal due to OH fragments generated in the photodissociation of CH_3COCH_2OH suggests that its dissociation rate (k) is $>10^8$ s^{-1}. A slow decay is observed afterwards due to the diffusion of the nascent OH fragments.

The rate of formation of the primary dissociation product OH, from the CH_3COCH_2OH molecules excited by a 248 nm photon, can be obtained by Rice–Ramsperger–Kassel–Marcus (RRKM) calculations. If the internal energy (E^*) of a molecule exceeds the dissociation energy E_0, the molecule is capable of spontaneous decomposition to fragments. The unimolecular decomposition rate $k(E^*)$ in a RRKM approximation [22] is described by the expression:

Table 1
Parameters used in RRKM calculations vibrational wavenumbers, cm^{-1}

Triplet CH_3COCH_2OH	Vibrational wavenumbers (cm^{-1})	
	Activated complex for the C–O bond scission	Activated complex for the C–C bond scission
3740, 2850(5), 1439(3), 1335(4), 1160, 1109, 1072, 948*(3), 790*, 484*, 349*(2), 245(2), 135, 82	As for molecule except those with asterisk replaced by 620, 570, 320, 260 and 1072 dropped to become reaction coordinate: $\log A\ (s^{-1}) = 14.6$, critical energy = 19.2 kcal mol^{-1}, reaction path degeneracy = 1, ratio of adiabatic partition functions $Q^{\dagger}/Q = 1.2$	As for molecule except those with asterisk replaced by 748, 590, 364, 249 and 1160 dropped to become reaction coordinate: $\log A\ (s^{-1}) = 14.38$, critical energy = 13.4 kcal mol^{-1}, reaction path degeneracy = 1, ratio of adiabatic partition functions $Q^{\dagger}/Q = 1.2$

$$k(E^*) = \frac{gQ^{\dagger}G(E^{\dagger} = E^* - E_0)}{QhN(E^*)}, \tag{3}$$

where $N(E^*)$ is the density of states for the molecule at E^*. $G(E^{\dagger})$ is the sum of state of critical configuration up to an excess energy $E^{\dagger}$, g is the reaction path degeneracy, and $Q^{\dagger}/Q$ is the ratio of adiabatic partition functions. Sums and densities of states are calculated by using the Whitten–Rabinovitch method [22]. A frequency factor of $\log A\ (s^{-1}) = 14.6$ can be extimated by comparison with the unimolecular dissociation of benzyl alcohol [23], which generates benzyl and OH radicals as products. A frequency factor of $\log A\ (s^{-1}) = 14.38$ is used by comparison with the unimolecular dissociation of acetone [24], which generates $CH_3 + COCH_3$ radicals as products. The vibrational frequencies of the triplet CH_3COCH_2OH are obtained from HF/6-31G** level calculation [25] (GAUSSIAN 92) of structural optimization and normal modes, which are corrected with a factor of 0.89. The C–O stretching mode at 1072 cm^{-1} and C–C stretching mode at 1160 cm^{-1} have become the reaction co-ordinates and four low frequency modes are adjusted until the agreement is reached between the A factor and the corresponding values calculated from the predicted entropy of activation. The frequencies taken for the activated complex and other parameters used in the RRKM calculations are given in Table 1. At the exitation energy corresponding to the 248 nm photon as 115 kcal mol^{-1}, the RRKM dissociation rate for the ground electronic state HA to $CH_3COCH_2 + OH$ is 10^4 s^{-1}. Similar to acetone, the triplet state of HA presumably have an energy minimum at 80 kcal mol^{-1}. After ISC the triplet CH_3COCH_2OH molecule is associated with an excess energy of 35 kcal mol^{-1}, which dissociates to $CH_3COCH_2 + OH$ by surpassing a barrier of 19.2 kcal mol^{-1}, with a RRKM rate of 1.5×10^{10} s^{-1}. The same calculation for the triplet CH_3COCH_2OH dissociation to $CH_3 + COCH_2$ OH or $CH_3CO + CH_2OH$ with a barrier of 13.4 kcal mol^{-1}, gives a RRKM rate of 2.7×10^{11} s^{-1}. This results in a quantum yield of about 2.7% for the OH channel. Although the lifetime of the triplet HA is estimated to be in the picosecond time scale, due existence to the bottleneck in the triplet formation, i.e., ISC rate, the observed OH formation rate would be corresponding to the ISC rate of 10^8 s^{-1}. However, further experiments are needed to verify the above estimations.

4. Conclusions

HA photoissociation has been demonstrated by excitation with a KrF excimer laser at 248 nm, generating CH_3COCH_2 and OH as products. The nascent OH radical is identified by LIF spectroscopy. The OH is formed with a modest rotational excitation equivalent to a rotational temperature of 450 ± 40 K, but with no vibrational excitation. No preferential OH formation in either spin doublets or Λ-doublets could be observed. By analysis of the OH rotational Doppler line-widths, the translational energy of the photofragments in the center of mass co-ordinate is found to be

8.7 ± 2.0 kcal mol^{-1}. The real time formation of OH, observed within the pump pulse duration, gives a dissociation rate of CH_3COCH_2OH to be $k \geqslant 10^8$ s^{-1}. The observation of OH with small amount of rotational energy, significant translational energy and a fast formation rate suggests that it is produced from the triplet excited CH_3COCH_2OH, following fast nonradiative transition (ISC) from the singlet $^1(n, \pi^*)$ excited hydoxyacetone.

Acknowledgements

The help of Dr. T.K. Ghanty performing the ab initio calculation is acknowledged. The authors wish to thank Dr. T. Mukherjee for his keen interest in this work. It was a pleasure to have a fruitful discussion with Dr. A.V. Sapre.

References

[1] J. Solomon, C. Jonah, P. Chandra, R. Bersohn, J. Chem. Phys. 55 (1971) 1908.
[2] G. Hancock, K.R. Wilson, in: Proceedings of the Fourth International Symposium on Molecular Beams, Cannes, France, 1973.
[3] D.J. Donaldson, S.R. Leone, J. Chem. Phys. 85 (1986) 817.
[4] S.W. North, D.A. Blank, J.D. Gezelter, C.A. Longfellow, Y.T. Lee, J. Chem. Phys. 102 (1995) 4447.
[5] S.K. Kim, S. Petersen, A.H. Zewail, J. Chem. Phys. 103 (1995) 477.
[6] J.C. Owrutsky, A.P. Baronavski, J. Chem. Phys. 110 (1999) 11206.
[7] J.J. Orlando, G.S. Tyndall, J.M. Fracheboud, E.G. Estupinan, S. Haberkorn, A. Zimmer, Atmos. Environ. 33 (1999) 1621.
[8] P.K. Chowdhury, H.P. Upadhyaya, P.D. Naik, J.P. Mittal, Chem. Phys. Lett. 351 (2002) 201.
[9] P.D. Naik, H.P. Upadhyaya, A. Kumar, A.V. Sapre, J.P. Mittal, Chem. Phys. Lett. 340 (2001) 116.
[10] P.K. Chowdhury, H.P. Upadhyaya, P.D. Naik, Chem. Phys. Lett. 344 (2001) 292.
[11] D.A. Hansen, E.K.C. Lee, J. Chem. Phys. 62 (1975) 183.
[12] R.A. Copeland, D.R. Crosley, Chem. Phys. Lett. 115 (1985) 362.
[13] A. Gandini, P.R. Hackett, J. Am. Chem. Soc. 99 (1977) 6195.
[14] H. Zuckermann, B. Schmitz, Y. Hass, J. Phys. Chem. 92 (1988) 4835.
[15] D. Liu, W.H. Fang, X.Y. Fu, Chem. Phys. Lett. 325 (2000) 86.
[16] D.F. McMillen, D.M. Golden, Annu. Rev. Phys. Chem. 33 (1982) 493.
[17] F. Zabel, S.W. Benson, D.M. Golden, Int. J. Chem. Kinetics 10 (1978) 295.
[18] D.R. Lide (Ed.), CRC Handbook of Chemistry and Physics, 80th edn., 1999–2000.
[19] S.W. Benson, Thermochemical Kinetics, Wiley, New York, 1976.
[20] G.H. Dieke, H.M. Crosswhite, J. Quant. Spectrosc. Radiat. Transfer 2 (1962) 97.
[21] J.L. Chidsey, D.R. Crosley, J. Quant. Spectrosc. Radiat. Transfer 23 (1980) 187.
[22] P.J. Robinson, K.A. Holbrook, Unimolecular Reactions, Wiley-Interscience, New York, 1972.
[23] P.K. Chowdhury, J. Phys. Chem. 98 (1994) 13112.
[24] M. Szwarc, J.W. Taylor, J. Chem. Phys. 23 (1955) 2310.
[25] M.J. Frisch et al., GAUSSIAN 92, Revision E 1, Gaussian, Inc, Pittsburgh, PA, 1992.